Controlling Semiconducting and Insulating States of SnO_2 Reversibly by Stress and Voltage

Kewei Liu,* Makoto Sakurai,* and Masakazu Aono*

International Center for Materials Nanoarchitectonics (MANA), National Institute for Materials Science (NIMS), Tsukuba 305-0044, Japan

ABSTRACT

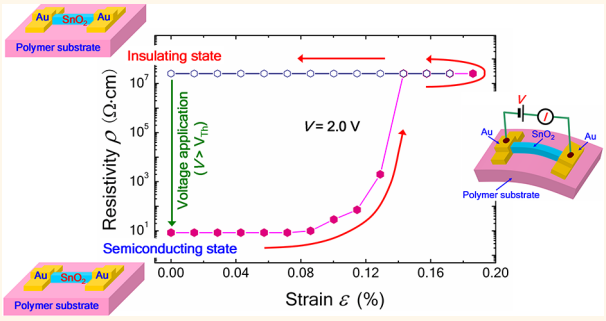

By applying mechanical stress (by bending a flexible substrate) and an appropriate voltage, the conductance of a single-crystal SnO_2 microrod on a flexible substrate can be tuned in a reversible and nonvolatile manner. The creation and elimination of lattice defects controlled by strain and electrical healing is the origin of this novel transition. A SnO_2 microrod changes continually from its normal semiconducting state to an insulating state by bending the flexible substrate. The insulating state is maintained even after straightening the substrate. Interestingly, by applying an appropriate voltage, the defects are electrically healed and the insulating state reverts to the original semiconducting state. The structural changes in the SnO_2 microrod observed in the Raman spectra are consistent with the nonvolatile property of the transport. This flexible SnO_2 device with the reversible and nonvolatile modification of electrical properties is expected to lead to a better understanding of the mechanism of defect creation and elimination and has potential application in novel flexible strain sensors and switches.

KEYWORDS: SnO_2 microrods · reversible · nonvolatile · defect creation and elimination · electrical properties · flexible strain sensors and switches

The most important characteristic of semiconductors used in electronic devices such as transistors, memories, and sensors is the controllability of the electrical properties over a wide range, either permanently or dynamically.[1] Doping with appropriate impurity atoms that act as electron donors or acceptors is an efficient approach to permanently tuning the electrical properties of semiconductors and to creating p−n junctions; this approach has been widely used in the semiconductor industry.[2] In addition, the electrical properties of semiconductors are often dynamically modified by the electrical field, temperature, illumination, and strain, leading to the development of a wide range of semiconductor devices including transistors,[3,4] photodetectors,[5−8] and piezodevices.[9,10] However, impurity doping is an irreversible process, while dynamical control is always carried out in a volatile manner. Therefore, reversible and nonvolatile tuning of the electrical properties of semiconductors will be a breakthrough in semiconductor device technology.

According to previous reports,[11−13] mechanical deformation or strain can induce defects, which in turn alter the electrical conductivity of a semiconductor material. In addition, some of these defects can be removed by electrical healing.[14,15] Therefore, the idea of using the ability to tune the conductivity by the creation and elimination of lattice defects in semiconductors may produce a novel reversible and nonvolatile transition of the conductivity. Recently, flexible and stretchable electronics, known as the technology that integrates electronic devices on flexible substrates, is becoming one of the most interesting research fields owing to its novel properties and wide applications in many fields.[16−20] In this study, we demonstrated the reversible and nonvolatile control of the resistivity of individual single-crystal SnO_2 microrods on a flexible polymer substrate for the first time. A SnO_2 microrod changes continuously from its normal semiconducting state to an insulating state owing to the creation of lattice defects upon applying mechanical stress (by bending the flexible substrate). Because of the inverse symmetry of the rutile structure of SnO_2, this transition is different from the strain-induced change in resistance in ZnO due to the piezoelectric effect,[21,22] which is reversible with the

* Address correspondence to Liukewei2007@yahoo.com.cn, Liu.Kewei@nims.go.jp (K.L.); Sakurai.Makoto@nims.go.jp (M.S.); Aono.Masakazu@nims.go.jp (M.A.).

Received for review May 25, 2012 and accepted July 11, 2012.

Published online July 11, 2012
10.1021/nn302312v

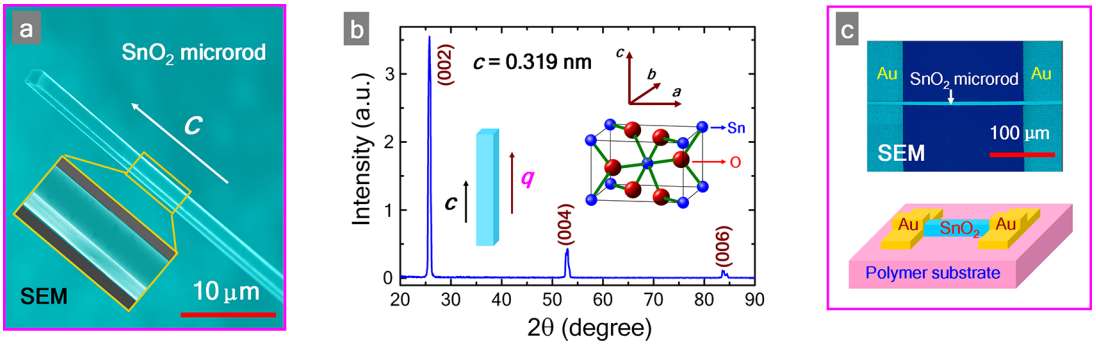

Figure 1. Structural characterization of SnO_2 microrods. (a) SEM image of an as-grown SnO_2 microrod with faceted structure. (b) XRD patterns of as-grown single SnO_2 microrod with scattering vector q parallel to rod axis. The inset shows the unit cell of the rutile structure of SnO_2. (c) Schematic illustration and SEM image of SnO_2 microrod device.

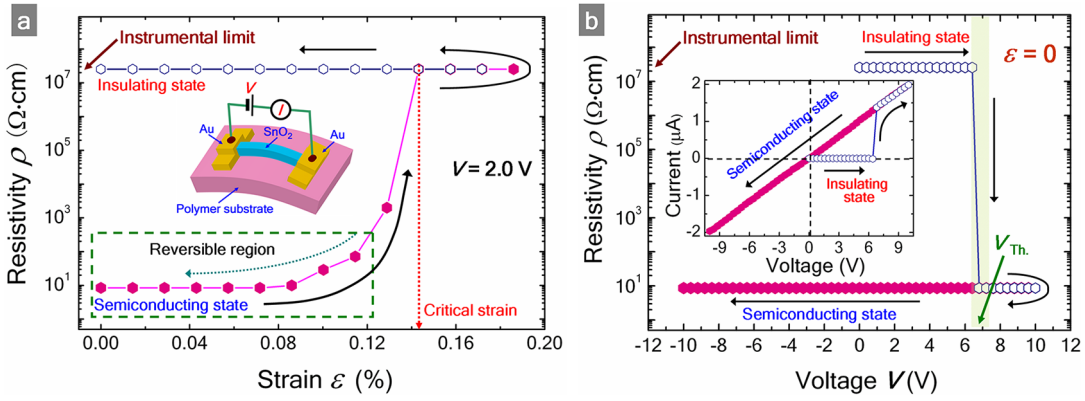

Figure 2. Electrical properties of SnO_2 microrods. (a) Resistivity of SnO_2 microrod device to mechanical strain at $V = 2.0$ V. The strain is increased from 0 to 0.186% (pink hexagons), then reduced to 0 (blue open hexagons). The inset shows a schematic illustration of the bent SnO_2 device. (b) Resistivity of SnO_2 microrod device to applied voltage. The applied voltage is increased from 0 to 10 V (blue open hexagons), then reduced to 0 V (pink hexagons). The inset shows the $I-V$ curves of the SnO_2 device in both the insulating and semiconducting states.

removal of strain. In the present work, the insulating state is maintained even after the strain is released (by straightening the flexible substrate) because residual defects are plastically formed. Interestingly, the application of an appropriate voltage can cause the insulating state to revert to the original semiconducting state. This simple and efficient control method of inducing a novel reversible and nonvolatile transition of the conductivity in semiconductors may pave the way for the development of novel strain sensors and switches with potential application in flexible electronics.

RESULTS AND DISCUSSION

Structure of Single-Crystal SnO_2 Microrods and Microrod Device. The SnO_2 microrods were synthesized by a simple thermal evaporation method (Figure S1).[23,24] Figure 1a shows a scanning electron microscope (SEM) image of an as-grown SnO_2 microrod. The microrods are well faceted and have square cross sections of side ~2 μm and uniform lengths of 3–5 mm. The X-ray diffraction (XRD) patterns from a single microrod with the scattering vector q parallel to the rod axis (Figure 1b) show that the SnO_2 microrods possess a single-crystal rutile structure (inset in Figure 1b) with the length direction along the tetragonal c-axis. Figure 1c shows a SEM image and a schematic illustration of a SnO_2 microrod device. A SnO_2 microrod lies horizontally on a flexible polymer film (Kapton) and is fixed using Au electrodes at both ends. The distance between the two Au electrodes is ~200 μm.

Reversible and Nonvolatile Conductance Transition. When the film is bent (inset in Figure 2a), tensile strain ε is induced in the SnO_2 microrod.[25] The resistance of the SnO_2 microrod was measured by applying a voltage (V) between the two Au electrodes at room temperature (Figure S2). The linear current–voltage ($I-V$) curves of the device indicate the formation of ohmic contacts between the Au electrodes and the microrod that are maintained under different strains (inset in Figure 2b and Figure S4). The as-grown SnO_2 microrods are n-type semiconductors because of their intrinsic impurities, such as oxygen vacancies, and their resistivity ρ is ~10 Ωcm. The state with this resistivity is referred to as the semiconducting state. Figure 2a shows the resistivity as a function of strain at V = 2.0 V. With increasing strain from 0 to ~0.12%, the resistivity increased slightly and the change induced by the application of stress was reversible. As the strain was

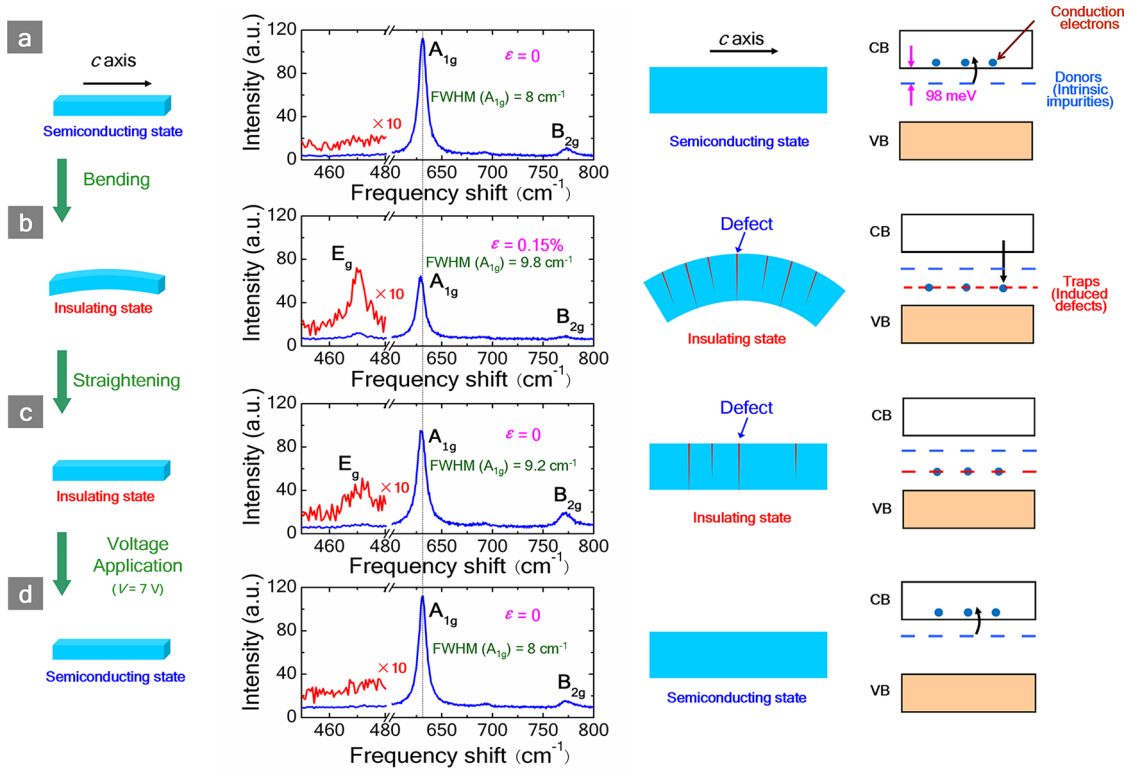

Figure 3. Schematic diagrams for the mechanism of transition between semiconducting and insulating states in SnO_2 microrod. The schematic structure, micro-Raman spectra, schematic crystal structure, and energy band diagram of the SnO_2 microrod are shown from left to right under different conditions: (a) Original straight SnO_2 microrod in semiconducting state. (b) After bending the SnO_2 microrod with a strain of 0.15%, the rod changed to the insulating state. (c) After straightening the SnO_2 microrod, the rod remained in the insulating state. (d) By applying a voltage across the SnO_2 microrod, the rod changed to the semiconducting state. CB and VB are the conduction and valence bands of SnO_2, respectively.

increased further, the resistivity increased sharply and reached the instrumental limit ($\sim 2 \times 10^7$ Ωcm) at a critical strain of ~0.14%. This state is referred to as the insulating state. This insulating state was maintained even when the strain was reduced to zero. Interestingly, the insulating state induced by a mechanical strain can be changed back to the semiconducting state by applying an appropriately large *V* (Figure 2b). Switching from the insulating state to the semiconducting state occurred at a certain threshold voltage (V_{Th}) of 6.5 ± 0.2 V. This semiconducting state was maintained even when the voltage was reduced to zero or an opposite voltage was applied. The corresponding *I*–*V* curves of the device are shown in the inset of Figure 2b. The results demonstrate the controllable, nonvolatile, and reversible resistance states of the SnO_2 microrod under the application of stress and voltage.

Structural Change in SnO_2 Microrod. To study the structural states of the SnO_2 microrod, we measured micro-Raman spectra with the measuring direction perpendicular to the *c*-axis. The Raman spectra of the straight microrods in the semiconducting state exhibit two Raman scattering peaks at 631 and 773 cm^{-1} (Figure 3a), corresponding to the A_{1g} and B_{2g} modes, respectively.[26,27] The E_g mode was not observed in the spectra obtained from the experimental configuration: the A_{1g} and B_{2g} modes in the SnO_2 crystal are attributed to the lattice vibrations in the plane perpendicular to the *c*-axis, while the E_g mode is attributed to the lattice vibrations parallel to the *c*-axis.[26,27] Unintentionally doped SnO_2 crystal is known as an n-type semiconductor because of its intrinsic impurities such as oxygen vacancies (Figure 3a and Figure S3).[28] When we bent the microrod (Figure 3b), the A_{1g} mode shifted to a lower frequency, which is related to the tensile strain along the *c*-axis.[29] The line width of the A_{1g} peak (fwhm (A_{1g})) increased from 8 cm^{-1} to 9.8 cm^{-1}, suggesting a decrease in the crystal quality upon the application of stress.[30] The E_g mode located at 471 cm^{-1} in the spectrum indicates the appearance of an area inclined to the *c*-axis in the bent microrod. Because the intensity of the E_g mode is much lower than those of the A_{1g} and B_{2g} modes, the inclined area is partially formed in the microrod. Planar defects therefore occur at the boundary of the inclined area, and these defects act as trapping centers for the conduction electrons (Figure 3b).[31] After straightening the rod (Figure 3c), the E_g peak was still observed, although its intensity had decreased to some extent. This result indicates that some of the inclined area had returned to its original state, but the rest remained inclined, and hence some of the defects

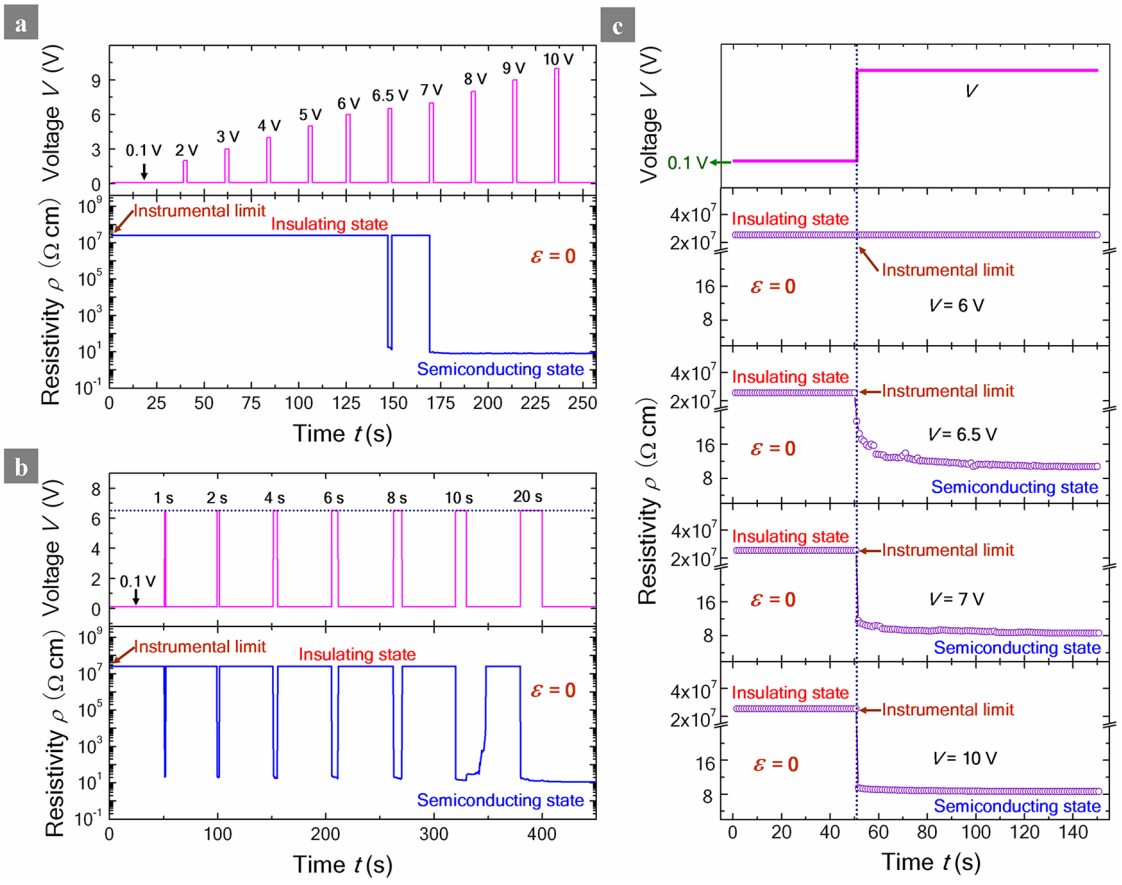

Figure 4. Dynamic change of resistivity in transition from insulating state to semiconducting state. (a) Resistivity as a function of pulse voltage applied to SnO_2 microrod device. (b) Change in resistivity induced by the application of pulse voltage (6.5 V) with different pulse widths of 1, 2, 4, 6, 8, 10, and 20 s. (c) Process of transition from insulating state to semiconducting state induced by continuously applying different voltages of 6, 6.5, 7, and 10 V.

remained and continued to trap the conduction electrons, as shown in the band diagram in Figure 3c. Also, fwhm (A_{1g}) slightly decreased to 9.2 cm^{-1}, indicating that crystal quality is still reduced. The A_{1g} peak shifted to a slightly higher frequency, but it did not return to its original position, suggesting that tensile strain still existed in the straight rod. This is consistent with the nonvolatile behavior observed in the transport measurement. When a voltage above V_{Th} was applied (Figure 3d), the defects, the inclined area, and the tensile strain were completely removed, which was confirmed by the disappearance of the E_g peak and the frequency shift and the decrease in line width of the A_{1g} peak in the Raman spectra, indicating that the quality of the crystal had recovered.

Mechanism of Transition from Semiconducting State to Insulating State. The above results indicate the following mechanism for the transition from the semiconducting state to the insulating state. The strain causes elastic lattice deformation and also creates some lattice defects (such as dislocations, stacking faults, and twin boundaries) in the microrod. According to the previous reports,[32−35] when the stress/strain was applied parallel to the *c*-axis of a rutile structure, the slip initially occurred on the {101}⟨101⟩ slip systems, and most of the dislocations in these systems formed long arrays with edge character that were parallel to [100] or [010]. Therefore, in our case, it is expected that the dislocations first appear on the top surface of the SnO_2 microrod upon bending. These defects can trap electrons,[31] inducing electrostatic potential barriers near the trapping sites (depletion region), and also reduce the mobility of electrons.[35] The application of stress leads to the change in the electron transport process. Because the defect density is very low in the case of a small strain, the resistivity increases slightly and the current still flows in the microrod. When the strain is reduced to zero, the resistivity returns to its original value because of the electrical removal of the defects (discussed later). With increasing strain, planar defects such as small-angle grain boundaries are formed.[36] The electron transport process is disrupted, and the microrod changes from the semiconducting state to the insulating state. Because no current flows in the insulating state, the defects cannot be healed after the strain is released, and the microrod thus remains in the insulating state. This change in resistivity is not caused by the piezoelectric field effect,[21,22] because SnO_2 is a

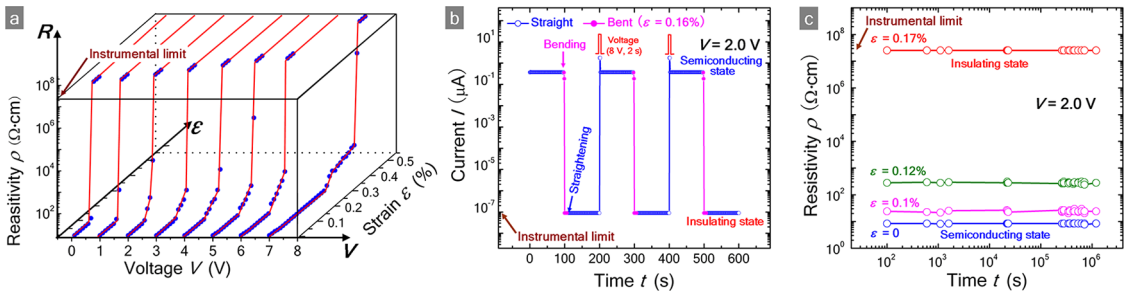

Figure 5. Electrical properties and switching behaviors of SnO_2 microrod. (a) Strain dependence of resistivity of SnO_2 microrod at different voltages. (b) Current response of device to periodic application of strain and voltage at V = 2.0 V. (c) Retention behavior of SnO_2 microrod with different resistance states at V = 2.0 V. The states are achieved by introducing different strains of 0 (blue), 0.1% (pink), 0.12% (green), and 0.17% (red).

non-piezoelectric material.[37,38] Also, the nonvolatile behavior relative to the strain excludes the possibility of the piezoelectric effect being caused by the broken structural symmetry of the bent SnO_2 microrod.[21,22]

We have excluded the effect of the Au-SnO_2 contacts in our explanation of the transition induced by stress and voltage for the following reasons. The deformation of the contacts caused by the application of stress may lead to the transition from the semiconducting state to the insulating state. The application of voltage promotes an electromigration process at the interface, resulting in the transition back to the semiconducting state. If the reversible change was caused by the change in the Au−SnO_2 contacts, the electric healing process would strongly depend on the polarity of the applied voltage because the electromigration would depend on the direction of the electric field. However, no polarity dependence was observed in this work (see Figure 2b). Additionally, ohmic contacts between the Au electrodes and the microrod are maintained under different strains (see Figure S4). Therefore, the effect of the Au−SnO_2 contacts on the transition could be excluded in the interpretation of the reversible and nonvolatile properties of SnO_2 microrods.

Dynamic Response of Resistivity. To further clarify the mechanism of the transition from the insulating state to the semiconducting state, the resistivity of the SnO_2 microrod was measured upon the application of voltage. When a pulse voltage from 2 to 6 V with a pulse width of 2 s was applied to the microrod in the insulating state, the resistivity did not change (Figure 4a). When the pulse voltage was increased to 6.5 V, the resistivity was markedly reduced during the application of voltage, but increased after the voltage was removed. This voltage is equal to $V_{Th.}$ (Figure 2b). The microrod changed from the insulating state to the semiconducting state with the application of a pulse voltage of 7−10 V. To further study the change in resistivity upon the application of $V_{Th.}$, 6.5 V pulses with different widths were then applied to the rod (Figure 4b). When the pulse width was less than 10 s, a large decrease in resistivity was observed only during the application of voltage. The low resistivity obtained at a pulse width of 10 s was unstable and increased slowly after the voltage was removed. When the pulse width was further increased to 20 s, the semiconducting state became stable. Figure 4c shows the transition processes under continuously applied voltages of 6, 6.5, 7, and 10 V. The voltages from 6.5 to 10 V caused the transition from the insulating state to the semiconducting state. The decay time of the resistivity decreases with increasing voltage.

Mechanism of Dynamic Response in Healing Process. The results shown in Figure 4 lead us to propose the following mechanism for the transition from the insulating state to the semiconducting state under the application of voltage. In the insulating state, electrons are trapped at the defect sites and form a depletion region. When a voltage is applied between the electrodes, the voltage markedly decreases in the depletion region and thus produces a strong electric field at the defect sites (Figure S5). The electric field reduces the trapping potential barrier, which is known as the Poole−Frenkel effect.[39] When the electric field reaches the threshold value, the trapped electrons are released to the conduction band and cause the depletion region to disappear, resulting in the flow of electrons. The rod is in the semiconducting state during the application of the electric field, but defects still exist in the rod and can retrap the electrons after the removal of the electric field, as shown in Figure 4b. With increasing pulse width or applied voltage, a local energy transfer from the electrons to the lattice (local Joule heating) occurs and induces the electrical healing of the defects.[15,40] The energy and frequency of the transfer increase with the voltage. However, because the thermal energy was transferred mainly to the electrodes and the substrate, we did not observe an increase in temperature (Figure S6).

Strain Sensing and Switching Properties of the Device. Figure 5a shows the strain dependence of the resistivity of the SnO_2 microrod under different applied voltages. The critical strain increases gradually with the voltage and changes markedly at V = 7 V. The increase in critical

strain with increasing applied voltage confirms that electrical healing of the defects occurred in the microrod in the reversible region (Figure 2a). The voltage dependence of the critical strain can be used to produce a new type of strain sensor. Figure 5b shows the reproducibility of the switching between the insulating and semiconducting states induced by the application of strain and voltage, respectively. Figure 5c depicts the retention behavior of the SnO_2 microrod with different resistance states at $V = 2.0$ V. The stability of each state under different values of applied strain demonstrates the possibility of multivalue recording, which may be required for future computer technologies.[41−43]

CONCLUSIONS

We have demonstrated a reversible and nonvolatile transition in the conductance of SnO_2 microrods by the creation and annihilation of lattice defects induced by mechanical stress and voltage. The transition between the semiconducting and insulating states is highly controllable, stable, and reproducible. Our results should stimulate future studies from the viewpoints of both fundamental science and device applications, and the reversible and nonvolatile mechanism is expected to be applied in strain sensors, switches, and memories for use in future flexible electronics.[16−20,41−44]

METHODS

Fabrication of the SnO_2 Microrods. The SnO_2 microrods were synthesized through a chemical vapor deposition process at 990 °C. To grow the SnO_2 microrods, a mixture of highly pure (99.999%) SnO_2 powder and (99.999%) graphite powder with a weight ratio of 1:1 SnO_2/C was used as the source. A ceramic boat containing the SnO_2/C powder was placed in a horizontal tube furnace (see Figure S1). The temperature was first raised to 200 °C in a vacuum for 10 min to remove the water and adsorption gas in the source. After that, we increased the temperature to 990 °C with a flow of highly pure argon mixed with 4% oxygen as the protective medium and carrier gas with a pressure of 9.0×10^2 Pa. The temperature was maintained for 60 min and then naturally cooled to room temperature. SnO_2 microrods with uniform lengths of 3−5 mm and cross-sectional squares of 1−2 μm on a side were grown at the end of the ceramic boat.

Analysis of the SnO_2 Microrods. The structural information of the SnO_2 microrods was obtained using SEM (Hitachi S-4800), Raman spectra (laser excitation at 514.5 nm), and XRD (Rigaku AFC7R, Mo Kα radiation, $\lambda = 0.7106$ Å). In the measurements of XRD, a single SnO_2 microrod was glued on a sharp glass rod to reduce background noise (accelerating voltage: 50 kV, current: 250 mA).

Fabrication and Electrical Properties of the SnO_2 Microrod Device. The SnO_2 microrod was first transferred from the ceramic boat to the Kapton substrate by using tweezers and a metal wire with a sharp tip. The microrod lies flat on the flexible substrate. The Au electrodes with a thickness of 500 nm were made by thermal evaporation though a shadow mask onto the substrate at room temperature. The current−voltage (I−V) and switching characteristics of an individual SnO_2 microrod-based device were measured in air using a picoammeter (Keithley, model 6458). A mechanical linear stage was used to bend the substrate. The measurement system is shown schematically in Figure S2.

Conflict of Interest: The authors declare no competing financial interest.

Acknowledgment. This work was supported in part by the World Premier International Research Center (WPI) Initiative on Materials Nanoarchitectronics, MEXT, Japan, and in part by JSPS KAKENHI (23560032). We thank Dr. Y. Michiue and Dr. A. Sato for measurement of the XRD.

Supporting Information Available: Additional information about methods and device properties. This material is available free of charge *via* the Internet at http://pubs.acs.org.

REFERENCES AND NOTES

1. Yu, P. Y.; Cardona, M. *Fundamentals of Semiconductors: Physics and Materials Properties*, 3rd ed.; Springer: Berlin, 2005; p 159.
2. Hall, R. N.; Dunlap, W. C. P-N Junctions Prepared by Impurity Diffusion. *Phys. Rev.* **2008**, *80*, 467–468.
3. Lee, M. L.; Fitzgerald, E. A.; Bulsara, M. T.; Currie, M. T.; Lochtefeld, A. Strained Si, SiGe, and Ge Channels for High-Mobility Metal-Oxide-Semiconductor Field-Effect Transistors. *J. Appl. Phys.* **2005**, *97*, 01101.
4. Schwierz, F. Graphene Transistors. *Nat. Nanotechnol.* **2010**, *5*, 487–496.
5. Razeghi, M.; Rogalski, A. Semiconductor Ultraviolet Detectors. *J. Appl. Phys.* **1996**, *79*, 7433–7473.
6. Liu, K. W.; Sakurai, M.; Aono, M. ZnO-Based Ultraviolet Photodetectors. *Sensors* **2010**, *10*, 8604–8634.
7. Liu, K. W.; Ma, J. G.; Zhang, J. Y.; Lu, Y. M.; Jiang, D. Y.; Li, B. H.; Zhao, D. X.; Zhang, Z. Z.; Yao, B.; Shen, D. Z. Ultraviolet Photoconductive Detector with High Visible Rejection and Fast Photoresponse Based on ZnO Thin Film. *Solid-State Electron.* **2007**, *51*, 757–761.
8. Liu, K. W.; Shen, D. Z.; Shan, C. X.; Zhang, J. Y.; Yao, B.; Zhao, D. X.; Lu, Y. M.; Fan, X. W. Zn0.76Mg0.24O Homojunction Photodiode for Ultraviolet Detection. *Appl. Phys. Lett.* **2007**, *91*, 201106.
9. Hu, Y.; Chang, Y.; Fei., P.; Snyder, R. L.; Wang, Z. L. Designing the Electric Transport Characteristics of ZnO Micro/Nanowire Devices by Coupling Piezoelectric and Photoexcitation Effects. *ACS Nano* **2010**, *4*, 1234–1240.
10. Boxberg, F.; Sondergaard, N.; Xu, H. Q. Photovoltaics with Piezoelectric Core-Shell Nanowires. *Nano Lett.* **2010**, *10*, 1108–1112.
11. Li, X.; Yang, W.; Liu, B. Bending Induced Rippling and Twisting of Multiwalled Carbon Nanotubes. *Phys. Rev. Lett.* **2007**, *98*, 205502.
12. Han, X. D.; Zhang, Y. F.; Zheng, K.; Zhang, X. N.; Zhang, Z.; Hao, Y. J.; Guo, X. Y.; Yuan, J.; Wang, Z. L. Low-Temperature *in Situ* Large Strain Plasticity of Ceramic SiC Nanowires and Its Atomic-Scale Mechanism. *Nano Lett.* **2007**, *7*, 452–457.
13. Golberg, D.; Bai, X. D.; Mitome, M.; Tang, C. C.; Zhi, C. Y.; Bando, Y. Structural Peculiarities of *in Situ* Deformation of a Multi-Walled BN Nanotube inside a High-Resolution Analytical Transmission Electron Microscope. *Acta Mater.* **2007**, *55*, 1293–1298.
14. Dager, M. D.; Creil, P.; Leyens, C.; van der Zwaay, S.; Schubert, U. S. Self-Healing Materials. *Adv. Mater.* **2010**, *22*, 5424–5430.
15. Zang, J.; Xu, Z.; Webb, R. A.; Li, X. Electrical Self-Healing of Mechanically Damaged Zinc Oxide Nanobelts. *Nano Lett.* **2011**, *11*, 241–244.
16. Kim, K. S.; Zhao, Y.; Jang, H.; Lee, S. Y.; Kim, J. M.; Kim, K. S.; Ahn, J.-H.; Kim, P.; Choi, J.-Y.; Hong, B. H. Large-Scale Pattern Growth of Graphene Films for Stretchable Transparent Electrodes. *Nature* **2009**, *457*, 706–710.
17. Rogers, J. A.; Someya, T.; Huang, Y. Materials and Mechanics for Stretchable Electronics. *Science* **2010**, *327*, 1603–1607.

18. Sekitani, T.; Noguchi, Y.; Hata, K.; Fukushima, T.; Aida, T.; Someta, T. A Rubberlike Stretchable Active Matrix Using Elastic Conductors. *Science* **2008**, *321*, 1468–1472.
19. Lipomi, D. J.; Vosgueritchian, M.; Tee, B. C-K.; Hellstrom, S. L.; Lee, J. A.; Fox, C. H.; Bao, Z. N. Skin-Like Pressure and Strain Sensors Based on Transparent Elastic Films of Carbon Nanotubes. *Nat. Nanotechnol.* **2011**, *6*, 788–792.
20. Lu, X.; Xia, Y. Buckling Down for Flexible Electronics. *Nat. Nanotechnol.* **2006**, *1*, 163–164.
21. Wang, Z. L.; Song, J. Piezoelectric Nanogenerators Based on Zinc Oxide Nanowire Arrays. *Science* **2006**, *312*, 242–246.
22. Wang, X.; Zhou, J.; Song, J.; Liu, J.; Xu, N.; Wang, Z. L. Piezoelectric Field Effect Transistor and Nanoforce Sensor Based on a Single ZnO Nanowire. *Nano Lett.* **2006**, *6*, 2768–2772.
23. Sakurai, M.; Wang, Y. G.; Uemura, T.; Aono, M. Electrical Properties of Individual ZnO Nanowires. *Nanotechnology* **2009**, *20*, 155203.
24. Liu, K. W.; Sakurai, M.; Liao, M. Y.; Aono, M. Giant Improvement of the Performance of ZnO Nanowire Photodetectors by Au Nanoparticles. *J. Phys. Chem. C* **2010**, *114*, 19835–19839.
25. Lee, K. J.; Lee, J.; Hwang, H.; Reitmeier, Z. J.; Davis, R. F.; Rogers, J. A.; Nuzzo, R. G. A Printable Form of Single-Crystalline Gallium Nitride for Flexible Optoelectronic Systems. *Small* **2005**, *1*, 1164–1168.
26. Peercy, P. S.; Morosin, B. Pressure and Temperature Dependences of the Raman-Acative Phonons in SnO_2. *Phys. Rev. B* **1973**, *7*, 2779–2786.
27. Diéguez, A.; Romano-Rodríguez, A.; Vilà, A.; Morante, J. R. The Complete Raman Spectrum of Nanometric SnO_2 Particles. *J. Appl. Phys.* **2001**, *90*, 1550–1557.
28. Chen, Z. W.; Lai, J. K. L.; Shek, C. H. Insights into Microstructural Evolution from Nanocrystalline SnO_2 Thin Films Prepared by Pulsed Laser Deposition. *Phys. Rev. B* **2004**, *70*, 165314.
29. Yoshikawa, M.; Katagin, G.; Ishida, H.; Ono, M.; Matsumura, K. Characterization of Crystalline Quality of Diamond Films by Raman Spectroscopy. *Appl. Phys. Lett.* **1989**, *55*, 2608–2610.
30. Ryu, S.; Maultzsch, J.; Han, M. Y.; Kim, P.; Brus, L. E. Raman Spectroscopy of Lithographically Patterned Graphene Nanoribbons. *ACS Nano* **2011**, *5*, 4123–4130.
31. McKenna, K. P.; Shluger, A. L. Electron-Trapping Polycrystalline Materials with Negative Electron Affinity. *Nat. Mater.* **2008**, *7*, 859–862.
32. Blanchin, M. G.; Fontaine, G. Transmission Electron Microscope Observations of Deformed Rutile (TiO_2). *Phys. Stat. us Solidi A* **1975**, *29*, 491–501.
33. Ashbee, K. H. G.; Smallman, R. E. The Plastic Deformation of Titanium Dioxide Single Crystals. *Proc. R. Soc. London A* **1963**, *274*, 195–205.
34. Ashbee, K. H. G.; Smallman, R. E. Stress-Strain Behavior of Titanium Dioxide (Rutile) Single Crystals. *J. Am. Ceram. Soc.* **1963**, *46*, 211–214.
35. Dominguez, J. E.; Fu, L.; Pan, X. Q. Effect of Crystal Defects on the Electrical Properties in Epitaxial Tin Dioxide Thin Films. *Appl. Phys. Lett.* **2002**, *81*, 5168–5170.
36. Dawson, I.; Bristowe, P. D.; Lee, M.-H.; Payne, M. C.; Segall, M. D.; White, J. A. First-Principle Study of a Tilt Grain Boundary in Rutile. *Phys. Rev. B* **1996**, *54*, 13727–13733.
37. Wang, Y. L.; Jiang, X. C.; Xia, Y. N. A Solution-Phase, Precursor Route to Polycrystalline SnO_2 Nanowires That Can Be Used for Gas Sensing under Ambient Conditions. *J. Am. Chem. Soc.* **2003**, *125*, 16176–16177.
38. Onuma, Y.; Wang, Z.; Ito, H.; Nakao, M.; Kamimura, K. Preparation and Piezoresistive Properties of Polycrystalline SnO_2 Films. *Jpn. J. Appl. Phys.* **1998**, *37*, 963–964.
39. Vincent, G.; Chantre, A.; Bois, D. Electric Field Effect on the Thermal Emission of Traps in Semiconductor Junctions. *J. Appl. Phys.* **1979**, *50*, 5484–5487.
40. Jin, C.; Suenaga, K.; Iijima, S. Plumbing Carbon Nanotubes. *Nat. Nanotechnol.* **2008**, *3*, 17–21.
41. Liao, L.; Fan, H. J.; Yan, B.; Zhang, Z.; Chen, L. L.; Li, B. S.; Xing, G. Z.; Shen, Z. X.; Wu, T.; Sun, X. W.; Wang, J.; Yu, T. Ferroelectric Transistors with Nanowire Channel: Toward Nonvolatile Memory Applications. *ACS Nano* **2009**, *3*, 700–706.
42. Waster, R.; Dittmann, R.; Staikov, G.; Szot, K. Redox-Based Resistive Switching Memories—Nanoionic Mechanisms, Prospects, and Challenges. *Adv. Mater.* **2009**, *21*, 2632–2663.
43. Hu, J.-M.; Li, Z.; Chen, L.-Q.; Nan, C.-W. High-Density Magnetoresistive Random Access Memory Operating at Ultralow Voltage at Room Temperature. *Nat. Commun.* **2011**, *2*, 553.
44. Liu, X.; Long, Y.-Z.; Liao, L.; Duan, X. F.; Fan, Z. Large-Scale Integration of Semiconductor Nanowires for High-Performance Flexible Electronics. *ACS Nano* **2012**, *6*, 1888–1900.